Biochemical and Structural Basis for Partially Redundant Enzymatic and Transcriptional Functions of DCoH and DCoH2[†,‡]

Robert B. Rose,*[,§] Kristi E. Pullen,[§] J. Henri Bayle,[||] Gerald R. Crabtree,[||] and Tom Alber[§]

Department of Molecular and Cell Biology, University of California, Berkeley, California 94720-3206, and Howard Hughes Medical Institute, Beckman Center for Molecular and Genetic Medicine, Stanford University, Stanford, California 94305

Received February 23, 2004; Revised Manuscript Received April 12, 2004

ABSTRACT: An inherited form of diabetes, maturity-onset diabetes of the young type 3 (MODY3), results from mutations in the transcriptional activator, hepatocyte nuclear factor-1α (HNF1α). Transcription by HNF1α is stimulated by the bifunctional coactivator DCoH (dimerization cofactor of HNF1). Strikingly, an *HNF1*α deletion in mice causes more severe phenotypes than a *DCoH* deletion. It has been hypothesized that a DCoH homolog, DCoH2, partially complements the *DCoH* deletion. To test this idea, we determined the biochemical properties and the 1.6-Å-resolution crystal structure of DCoH2. Like DCoH, DCoH2 forms a tetramer, displays pterin-4α-carbinolamine dehydratase activity, and binds HNF1α in vivo and in vitro. DCoH and DCoH2 adopt identical folds with structural differences confined largely to the protein surfaces and the tetramer interface. In contrast to the hyperstable DCoH tetramer, DCoH2 readily disproportionates and forms a 2:2 complex with HNF1 in vitro. Phylogenetic analysis reveals six major subfamilies of DCoH proteins, including unique DCoH and DCoH2 branches in metazoans. These results suggest distinct roles for DCoH and DCoH2. Differences in conserved surface residues could mediate binding to different effectors. We propose that HNF1α binding kinetics may distinguish regulation by DCoH2, under thermodynamic control, from regulation by DCoH, under kinetic control.

DCoH[1] is a small, conserved protein that functions both as a transcriptional co-activator and a metabolic enzyme. The pterin-4α-carbinolamine dehydratase (PCD) activity of DCoH helps to recycle tetrahydrobiopterin, a cofactor for the amino acid hydroxylases and nitric oxide synthase (*1, 2*). Mutations in DCoH in humans cause a rare form of hyperphenylalaninemia (*3, 4*), and loss of enzymatic activity is associated with the pigmentation disorder vitiligo (*5*). DCoH also associates with the transcriptional activators HNF1α and HNF1*β* and stimulates HNF1 activity (*6*). Mutations in HNF1α cause a monogenic form of diabetes, maturity onset diabetes of the young type 3 (MODY3) (*7*). Two MODY3 mutations disrupt the interaction with DCoH, as well as HNF1α dimerization (*8*). Recently, DCoH has been reported to be overexpressed in colon cancer carcinomas (*9*) and malignant melanomas (*10*).

Structural studies indicated that the mammalian DCoH exists in two oligomerization states in its nuclear and cytoplasmic forms (*1*). Cytoplasmic DCoH forms a tetramer consisting of two saddle-shaped dimers (*11*). The tetramer is enzymatically active, with an independent active site in each monomer (*12*). In the nucleus, DCoH forms a 2:2 complex with HNF1 proteins (*6*). The structure of the DCoH dimer bound to the HNF1α dimerization domain demonstrated that DCoH tetramerization and HNF1 binding are mediated by the same surface. This shared site implies that HNF1α competes with DCoH homotetramerization to interact with DCoH (*13*). The DCoH tetramer is hyperstable, and this stability explains the required cofolding of DCoH and HNF1α to form the 2:2 complex (*14*, *15*).

Despite the concerted functions of the HNF1α/DCoH complex, deletions of these genes in mice produce different phenotypes. HNF1α null mice display hyperphenylalaninemia, Laron-type dwarfism, and early onset diabetes mellitus (*16*−*18*). In contrast, DCoH null mice exhibit hyperphenylalaninemia, a predisposition to cataract formation, and only mild disruption of HNF1α function (*19*). This relatively mild syndrome led to a search of the mouse genome sequence for DCoH homologues that might partially complement the loss of the DCoH protein. This search identified the sequence of DCoH2, which shows 68% sequence identity to DCoH (also referred to as DCoH1 in this paper). DCoH2 orthologs also have been reported in chickens (*20*) and humans (*21*).

The sequence similarities of DCoH1 and DCoH2 suggested that they share similar biochemical properties. Here

[†] This work was supported by N. I. H. Grant GM54793. R.B.R. was supported by postdoctoral fellowships from the N. I. H. and the Juvenile Diabetes Foundation International.

[‡] Coordinates and structure factors for wild-type DCoH2 were deposited in the RCSB Protein Data Bank under entry code 1RU0.

* To whom correspondence should be addressed. Present address: Department of Biochemistry, 128 Polk Hall, North Carolina State University, Raleigh, NC 27695-7622. Phone: (919) 513−4191. Fax: (919) 515−2047. E-mail: bob_rose@ncsu.edu.

[§] University of California, Berkeley.

[||] Stanford University.

[1] Abbreviations: α (used as a prefix before a protein name), indicates an antibody for the protein; CHO, chinese hamster ovary; DCoH, dimerization cofactor of HNF1; EMSA, electromobility shift assay; FKBP, FK506-binding protein; HA, hemagglutinin; HNF1, hepatocyte nuclear factor-1; IP, immunoprecipitation; MODY, maturity-onset diabetes of the young; NCBI, National Center for Biotechnology Information; NOS, nitric oxide synthase; PAH, phenylalanine hydroxylase; PBS, phosphate-buffered saline; PCD, pterin-4α-carbinolamine dehydratase; PEG, poly(ethylene glycol); rmsd, root-mean-square deviation; SDSC, San Diego Super Computer; V_m, specific volume.

10.1021/bi049620t CCC: $27.50
Published on Web 05/21/2004

we test this idea by comparing the structures and activities of DCoH1 and DCoH2. Phylogenetic analysis of the DCoH family shows that these proteins represent the only two subfamilies of DCoH proteins in vertebrates. We show that DCoH2 mediates the same enzymatic and coactivator activities as DCoH1 but with different surface residues and different requirements for binding HNF1α in vitro. We propose that these differences may contribute to distinct mechanisms of regulation of HNF1 function.

EXPERIMENTAL PROCEDURES

DCoH2 Purification. Mouse DCoH2 cDNA was subcloned into a pGEX-2T vector (Pharmacia) and expressed in *Escherichia coli* BL21(DE3) cells (Stratagene). Cells were grown at 37 °C, harvested, and sonicated in phosphate-buffered saline (PBS) at pH 7.0. After centrifugation, the supernatant was loaded onto a glutathione affinity column (Pharmacia) preequilibrated in PBS. After extensive washing with PBS, DCoH2 was eluted by adding thrombin directly to the column and eluting according to the manufacturer's instructions. DCoH2 was further purified using an FPLC 15Q cation-exchange column (Pharmacia) preequilibrated in PBS. The protein was eluted with a 0−1 M NaCl gradient. A collodion concentrator (Schleicher & Schuell) was used to concentrate and buffer-exchange the protein into PBS.

Analytical Ultracentrifugation. Protein samples (50−70 μM in PBS) were centrifuged in a Beckman X-LA centrifuge at 15 000 rpm at 25 °C for 40 h to reach equilibrium. Absorbance data were fit to a model containing a single species. The observed small, random residuals validated this assumption.

Bacterial Complementation Assay. *E. coli* strain JP2255 *thiA*, *aroC*, *pheA*, *tyrA* was transformed with pJMZ3a (expressing *Pseudomonas aeruginosa* PhhA (phenylalanine hydroxylase) and PhhB (PCD/DCoH) in cis from the phh operon), pJMZ4 (PhhB alone), or pJMZ5 (PhhA alone)). pMB1 was derived from pACYC184 (New England Biolabs) expressing the PhhA gene from pJMZ5 (*22*). This plasmid has a non-ColE1 origin of replication and imparts chloramphenicol resistance. DCoH1 and DCoH2 were inserted into the Bluescript cloning vector downstream of a Lac promoter (pBS−DCoH). A Shine−Dalgarno sequence was added to increase translation efficiency. JP2255/pMB1 was transfected with pJMZ4 (*phhB* alone) or with pBS-DCoH1, pBS-DCoH2, or pBS-DCoH1 mutated at the active site for PCD activity (His63Leu (*15*)). Transformants were selected for tyrosine prototrophy on minimal media agar plates containing M9 salts, glucose, thiamine, and phenylalanine.

Electrophoretic Mobility Shift Assays. Nuclear extracts from transfected CHO cells were prepared by the method of Lassar (*23*). Gel shift assays were performed as described using a labeled oligonucleotide derived from the human albumin promoter (*19*). Truncated HNF1α (residues 1−280) was subcloned into the pQE-60 expression vector (Qiagen) in-frame with the C-terminal 6-His tag and purified according to the manufacturer's instructions (HNF1αtr-His). For mixed oligomer experiments, 10 ng of HNF1αtr-His was mixed with the nuclear extract on ice for 30 min prior to the addition of the oligonucleotide.

Immunoprecipitation of DCoH2 Complexes. CHO cells (lacking expression of either HNF1 or DCoH) were grown on plates in RPMI 1640 media supplemented with 10% fetal calf serum and antibiotics. All proteins were derived from the pBJ5 plasmid in which expression is directed by the SRα promoter. FLAG-tagged DCoH1 and DCoH2 with a 5′-tag (FLAG−DCoH) were generated as previously described (*19*). FKBP−DCoH1 is a fusion between the 12 kD human FK506-binding protein (FKBP) cDNA at the 5′ end of the DCoH cDNA yielding an amino-terminal fusion lacking a FLAG tag. Mouse HNF1α was fused to a C-terminal nine amino acid hemagglutinin (HA) tag (HNF1α-HA). HNF1αΔ-dim-HA lacks the amino terminal 32 amino acids of the HNF1α dimerization domain and retains the HA tag (*6*). Electroporations were preformed as described (*19*). Forty-eight hours posttransfection, cells were lysed on ice in TNEN (50 mM Tris-HCl, pH 7.4, 150 mM NaCl, 5 mM EDTA, 0.5% NP-40, 1 mM PMSF, 1 mM leupeptin, 1 mM pepstatin). Samples (30−100 mg protein) were incubated overnight at 4 °C with 2 mg of M2 antibody (Kodak), IgG1 isotype control (Becton Dickenson), or 12CA5 (0.1 mL (net) of ascites fluid) and 5−10 mL of 50% slurry of protein-G Sepharose. Western blots were performed as described (*19*) except 2 mg/mL M2 antibody was used to develop the anti-FLAG Western blot.

Affinity Chromatography Assay. The N-terminal 280 residues of mouse HNF1α were subcloned into pET24b (Novagen) with a His_6 tag added at the C-terminus (HNF1αtr-His). This construct retains the DNA-binding elements of HNF1α, including the dimerization and DNA-binding domains (*24*). The protein was expressed in *E. coli* BL21 cells and purified from cell lysate in PBS using a Ni^{2+}-chelating resin (Pharmacia). The fractions containing HNF1α were loaded onto a 15Q ion-exchange resin (Pharmacia) preequilibrated in PBS and eluted with a 0.15−1 M NaCl gradient. Further purification was achieved using gel filtration on a S300 column (Pharmacia) equilibrated with PBS. Interaction between DCoH2 and HNF1α was measured with His-tagged HNF1α immobilized on Ni^{2+}-chelating resin. Beads (30 μL) were equilibrated in PBS and loaded with 100 μg of purified His_6-tagged HNF1α. The beads were washed extensively in PBS containing 30 mM imidazole. Purified DCoH1 or DCoH2 (100 μg) was added to the beads and incubated for 45 min. The beads were washed three times with 1 mL of PBS plus 30 mM imidazole and mixed with 30 μL of 2× SDS loading buffer. This reaction (20 μL) was separated using SDS PAGE and visualized with Coomassie Blue (Sigma).

DCoH2 Structure Determination. DCoH2 (∼10 mg/mL) was crystallized in 10% 2-propanol, 0.1 M Na Hepes pH 7.5, and 20% PEG 4000 by hanging-drop vapor diffusion at 4 °C. The crystals were frozen in liquid nitrogen in mother liquor containing 10% PEG 400 as a cryoprotectant.

Data were collected at the Advanced Light Source and indexed with MOSFLM (*25*) using the ELVES interface (Table 1) (*26*). The data were scaled with Scala, and *F*'s were calculated with Truncate (*27*−*29*). The structure was solved by molecular replacement using a search model containing a DCoH dimer with residues differing between DCoH1 and DCoH2 replaced by alanines. After the rotation and translation search at 8−4 Å using CNS (*30*), the initial correlation coefficient was 0.62. After rigid body refinement, the *R*-factor was 44% for all data from 30 to 2 Å resolution. Starting with these phases, the model was rebuilt using ARP/

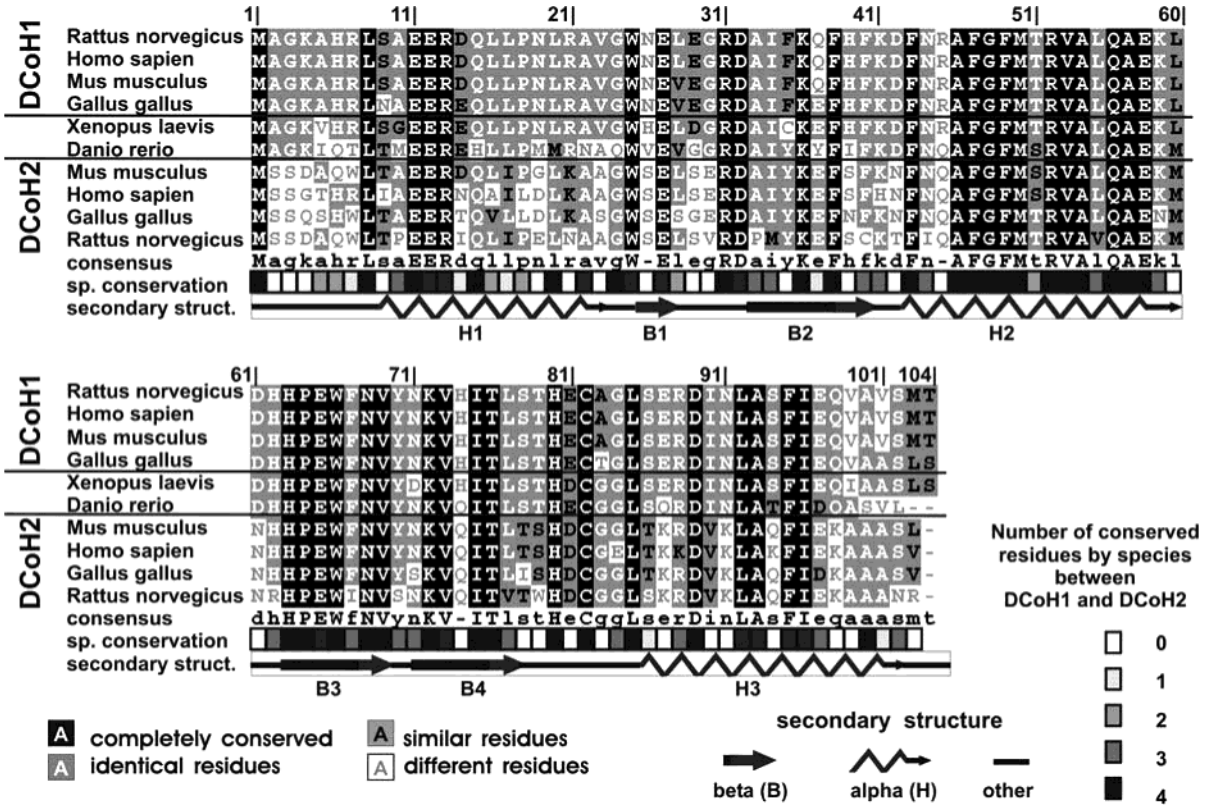

FIGURE 1: Alignment of vertebrate DCoH sequences. The DCoH1 and DCoH2 sequences of human, mouse, rat, and chicken were identified from a PSI-BLAST search of the nonredundant database. A single DCoH sequence was identified in frog (*Xenopus laevis*) and zebrafish (*Danio rerio*). Sequences were aligned with ClustalW (*37*). The figure was drawn using Boxshade (Hofmann, K., and Baron, M. D., http://workbench.sdsc.edu) with a similarity threshold of 50% using the default similarities (FYW, IVLM, RK, DE, GA, TS, NQ). Conservation between DCoH1 and DCoH2 (species conservation) is depicted on a scale from white to black by counting the number of identical residues between paralogs: white signifies no conservation, black signifies identical residues between DCoH1 and DCoH2 of all species. Light regions indicate divergence between DCoH paralogs.

Table 1: Data Collection and Refinement Statistics for DCoH2

Data	
space group	$P3_121$
unit cell length (Å)	$a = b = 57.92$; $c = 114.63$
resolution range (Å)	50−1.6
observations	141 185
unique reflns	30 110
completeness (%)	
50.0−1.60 Å	99.9
1.69−1.60 Å	99.9
$R_{sym}(I)$[a] (%)	
50.0−1.60 Å	6.6
1.69−1.60 Å	25.3
$\langle I\rangle/\langle\sigma(I)\rangle$	
50.0−1.60 Å	12.5
1.69−1.60 Å	3.8
Refinement	
residues in asymmetric unit	198[c]
water molecules	170
resolution range (Å)	50−1.6
σ cutoff [$\sigma(F)$]	0.0
R	0.215
R_{free}[b]	0.236
RMS deviations from ideal geometry	
bonds (Å)	0.005
angles (deg)	1.20

[a] $R_{sym} = \sum|I - \langle I\rangle|/\sum\langle I\rangle$. [b] Based on 1508 reflections (5% of the data). [c] Residues 1−3 of each monomer and residues 102 and 103 of monomer B are not visible in the structure.

wARP (*31*, *32*). Final rounds of refinement were accomplished using CNS alternated with manual model building using the program O (*33*). The model included 198 amino acids and 163 water molecules. Residues 1−3 of each monomer and residues 102−103 of one monomer were disordered and omitted from the final model. CNS was used to calculate buried surface area.

Phylogenetic Analysis. DCoH homologues were identified using PSI-BLAST (*34*) with the human DCoH2 sequence as the query. Five iterations were performed until no new sequences with *e*-values < 0.001 were identified. Forty-two distinct sequences from the nonredundant database at the National Center for Biotechnology (NCBI) were retrieved. Fewer orthologs were identified using the human DCoH1 sequence as the query. A phylogenetic tree was constructed using the PHYLIP Phylogeny Inference Package (*35*) implemented at the San Diego Super Computer Center (http://workbench.sdsc.edu). The tree was manually manipulated to eliminate branch crossings while preserving branch length and connectivity.

DCoH homologues in the human genome were identified using tblastn at the website of the NCBI. Searches were conducted using the human DCoH1 and DCoH2 sequences. Exon boundaries were identified using Genscan (*36*).

RESULTS

Alignment of the amino acid sequences of DCoH proteins from human, mouse, rat, and chicken revealed that the sequences could be clustered into two classes that define DCoH paralogs (Figure 1). The sequence of human DCoH2 is 61% identical to human DCoH1 and 88% identical to

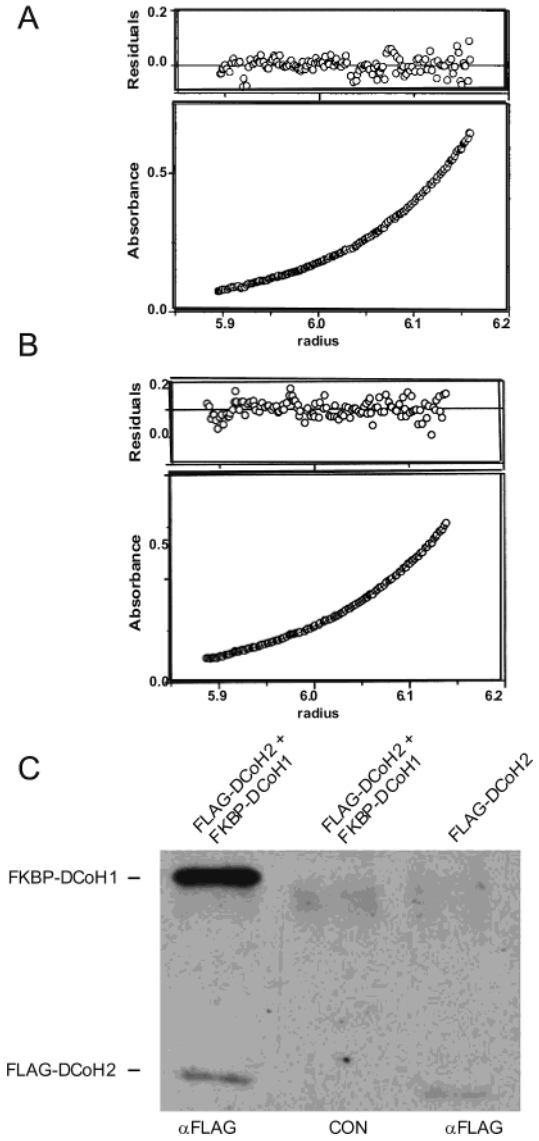

FIGURE 2: DCoH2 forms homotetramers in solution and heterotetramers with DCoH1. Shown in panel A, the apparent molecular weight of DCoH2 in solution was 49.8 kDa as determined by analytical ultricentrifugation at 50 μM concentration. This value is close to that predicted for a tetramer (47.2 kDa). The absorbance distribution was fit with a single exponential (bottom), and the residuals were distributed randomly about zero (top), indicating a good fit to the model. As seen in panel B, by comparison, the apparent molecular weight of DCoH1 (70 μM) was 44.9 kDa; the predicted value for a tetramer is 48 kDa. The random distribution of the residuals (top) indicated a good fit of the data (bottom) to a single exponential. Panel C shows that DCoH1 and DCoH2 can form hetero-oligomers. CHO cells were transfected with FLAG−DCoH2, an FKBP−DCoH1 fusion construct or both as indicated. Lysates were immunoprecipitated with the M2 (αFLAG) antibody or an isotype control antibody (CON). Western blots were carried out with rabbit αDCoH antiserum, which reacts with DCoH1 more strongly than with DCoH2.

mouse DCoH2. Rather than reflecting random drift of a duplicated gene, the evolutionary conservation of DCoH2 implies that DCoH2 and DCoH1 may perform distinct functions.

Mouse DCoH2 was expressed and purified to compare its properties with those of DCoH1. Analytical ultracentrifucation demonstrated that both DCoH1 and DCoH2 form tetramers in solution (Figure 2A,B). DCoH1 and DCoH2 share extensive similarity in helix 2, the recognition helix for HNF1 binding and DCoH homotetramerizartion. To address whether the two DCoH proteins can form hetero-oligomers, DCoH2 was fused to an N-terminal FLAG tag and coexpressed in CHO cells with a DCOH1 N-terminal fusion to FKBP. Immunoprecipitation of DCoH2 co-immunoprecipitated FKBP-DCoH1 indicating that mixed oligomers formed in vivo (Figure 2C).

P. aeruginosa encodes a phenylalanine hydroxylase, PhhA, and a DCoH homolog, PhhB (*22*). The PCD activity of PhhB is essential for growth on minimal medium (*38*). Expression of *phhA* and *phhB* can complement *E. coli* deficient in tyrosine biosynthesis, but deletion of *phhB* makes the strain auxotrophic for tyrosine. The loss of *phhB* was complemented by *DCoH1* or *DCoH2* but not the enzymatically inactive, His63Leu DCoH1 mutant (Figure 3A). This complementation implies that DCoH1 and DCoH2 exhibit similar PCD activities. This enzymatic activity is consistent with the nearly complete conservation of residues in the enzyme active site.

The mild reduction of HNF1α activity in DCoH1 null mice and the biochemical observation of a complementing activity (*19*) strongly implied that DCoH2 could bind and stabilize HNF1α dimers. We used several assays to test the ability of DCoH2 to bind to HNF1α in vivo and in vitro. Both DCoH proteins bound to HNF1α when the proteins were coexpressed in vivo (Figure 3B,C). Gel mobility shift assays of HNF1α and FLAG-tagged DCoH1 in nuclear extracts of transfected CHO cells revealed an HNF1α complex that could be supershifted with a mouse anti-DCoH1 polyclonal antibody or anti-FLAG tag antibodies (Figure 3B). HNF1α/DNA complexes containing FLAG-tagged DCoH2 were only supershifted with anti-FLAG antibodies, because the mouse polyclonal antibody is specific for DCoH1 (*19*). DCoH1 and DCoH2 binding to HNF1α required the N-terminal dimerization domain of HNF1α (Figure 3C) (*6*)

DCoH2 also bound HNF1α in vitro. In a gel mobility shift assay, a mixture of purified DCoH2 and HNF1α supershifted the HNF1α/DNA complex (Figure 3D). In contrast, purified DCoH1 did not efficiently supershift the HNF1α/DNA complex, consistent with the idea that the high stability of the DCoH1 tetramer inhibits complex formation with HNF1α (*8*). Similarly a glutathione-S-transferase (GST) pull-down assay demonstrated that purified DCoH2 protein but not DCoH1 bound efficiently to a column loaded with a large fragment (1−280) of HNF1α encompassing the dimerization, linker, and DNA-binding domains (Figure 3E). These results are consistent with previous work showing that DCoH1 does not readily interact with HNF1α upon mixing (*14, 15*) but folds together when the two proteins are coexpressed (*6*) or when DCoH1 and the HNF1α dimerization domain are renatured together from guanidinium hydrochloride (*8*).

DCoH proteins are thought to stimulate transcription by stabilizing HNF1α dimers (*6*). We tested the ability of DCoH2 to stabilize HNF1α dimers by measuring the exchange of monomers in preformed HNF1α dimers (Figure 3F). Full-length HNF1α was expressed in the presence or absence of DCoH1 or DCoH2. HNF1α dimers were challenged by mixing cell extracts with truncated HNF1α (HNF1αtr), which forms complexes that migrate more rapidly in gel-shift experiments. In the absence of DCoH proteins, HNF1α dimers exchanged readily with the challenging HNF1αtr, resulting in a band of intermediate

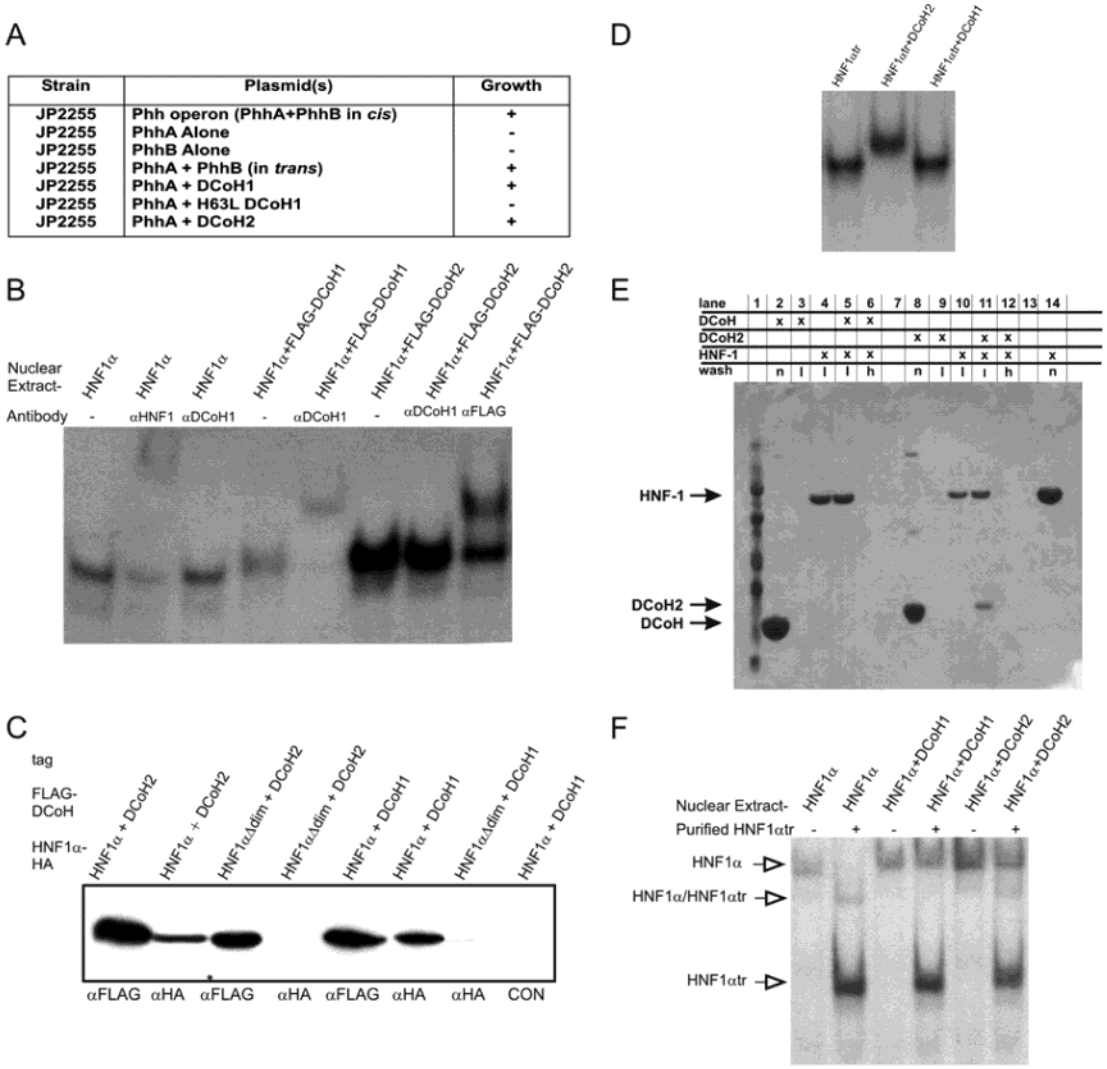

FIGURE 3: DCoH2 is a pterin-4α-carbinolamine dehydratase and interacts with HNF1α in vitro and in vivo. As seen in panel A, DCoH2 exhibits pterin-4α-carbinolamine dehydratase (PCD) activity. DCoH1 and DCoH2 complement a mutation in the *E. coli* PCD ortholog, *PhhB*. Complementation was assayed in a tyrosine auxotroph of *E. coli* strain JP2255 with the phh operon of *P. aeruginosa*. PhhA encodes phenylalanine hydroxylase. JP2255 includes the following genotype: *thiA, aroC, phe A, tyr A.* Growth was assayed on minimal media supplemented with phenylalanine and thiamine. The His63Leu mutation inactivates the dehydratase activity of DCoH1 (*15*). In panel B, gel mobility shift assays demonstrate that DCoH2 interacts in vivo with HNF1α. Assays were performed with an HNF1α binding site oligonucleotide and nuclear extracts prepared from CHO cells cotransfected with HNF1α and either DCoH1 or FLAG−DCoH2 as indicated. Antibodies (e.g., αHNF1) were included as indicated to supershift the DNA−protein complexes. Note that the HNF1α/DCoH2 complex was supershifted with the M2 antibody (directed to the FLAG tag on DCoH2, lane 8) but not a murine polyclonal antibody to DCoH1 that appears to lack specificity for DCoH2 (lane 7). The HNF1α/DCoH1 complex was supershifted with the antibody to DCoH1 (lane 5). Panel C shows that DCoH2 binds to the dimerization domain of HNF1α. Lysates were prepared from CHO cells cotransfected with HA-tagged HNF1α or HNF1αΔ1−32 (HNF1αΔdim) and FLAG-tagged DCoH1 or DCoH2 as indicated. Immunoprecipitations were performed with M2 antibody (directed to the FLAG tag on DCoH, lanes 1, 3, and 5) or 12CA5 (directed to the HA tag on HNF1α, lanes 2, 4, 6, and 7) or an unrelated rabbit antibody (CON, lane 8). DCoH proteins in the immunoprecipitates were analyzed by Western blot with the M2 (αFLAG) antibody. DCoH2 (lane 2) and DCoH1 (lane 6) coimmunoprecipitate with full-length HNF1α but not with HNF1α with the dimerization domain deleted (lanes 4 and 7). As shown in panel D, DCoH2, but not DCoH1, binds the HNF1α/DNA complex in vitro. The size of the HNF1α/DNA complex in the presence and absence of DCoH1 and DCoH2 was measured with an electrophoretic mobility shift assay. DCoH2 (lane 2), but not DCoH1 (lane 3), retarded the HNF1α/DNA complex. DNA binding assays were performed with 10 ng of purified recombinant HNF1α (HNF1αtr, truncated at amino acid 280). Purified recombinant DCoH (50 ng) was included in the indicated reactions. As shown in panel E, DCoH2 binds reversibly to HNF1α. Nickel sepharose beads were loaded with His_6-tagged HNF1α (residues 1−280), and either purified DCoH2 or DCoH1 was added. After being washed in low or high imidazole buffers, the beads were loaded onto an SDS−polyacrylamide gel: (lane 1) molecular weight standards; (lane 2) purified DCoH1; (lane 3) DCoH1 loaded on nickel sepharose beads lacking HNF1α; (lane 4) nickel sepharose beads loaded with HNF1α; (lane 5) DCoH1 loaded on beads preloaded with HNF1α; (lane 6) beads loaded with HNF1α after 250 mM imidazole wash; (lane 8) purified DCoH2; (lane 9) DCoH2 loaded on nickel sepharose beads lacking HNF1α; (lane 10) nickel sepharose beads loaded with HNF1α; (lane 11) DCoH2 loaded on beads preloaded with HNF1α; (lane 12) beads loaded with HNF1α after 250 mM imidazole wash; (lane 14) purified HNF1α. Abbreviations in the "wash" row are as follows: n, no wash; l, low (30 mM) imidazole wash; h, high (250 mM) imidazole wash. DCoH2 binds efficiently to HNF1α (lane 11). In contrast, purified DCoH1 fails to bind HNF1α in vitro in the absence of denaturants (Lane 5 and refs *14* and *15*). Panel F shows the stabilization of HNF1α dimerization by DCoH2 in vitro. HNF1α dimers formed in CHO cells were challenged by addition of purified, truncated HNF1α (HNF1αtr) and assayed by EMSA. In the absence of DCoH1 or DCoH2, HNF1αtr readily formed a mixed oligomer with HNF1α that displayed intermediate mobility (lane 2). Cotransfection of DCoH1 or DCoH2 inhibited the formation of mixed oligomers in the nuclear extract challenged with HNF1αtr.

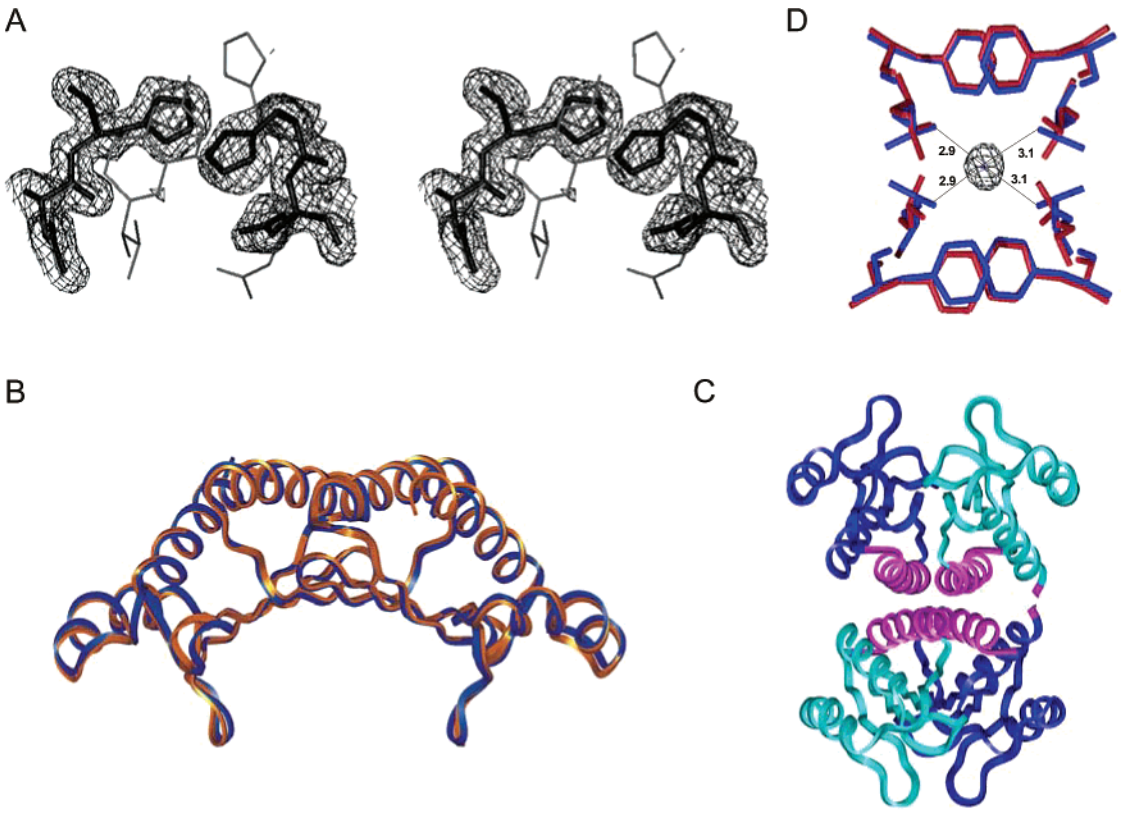

FIGURE 4: Structure of DCoH2. Panel A shows a stereodiagram of active site residues. The model of DCoH2 (thick sticks) is shown with the final, 1.6-Å-resolution, $2F_o - F_c$ electron density. Superimposed are the corresponding residues from DCoH1 (thin sticks) in complex with the product analogue 7,8-dihydrobiopterin (*12*). The two structures were superimposed using the Cα atoms of the active site residues (residues 58, 61−63, 78, 80−81, 89) with a rmsd of 0.47 Å (wall-eyed stereo). As shown in panel B, DCoH2 (blue) and DCoH1 (orange) dimers adopt the same fold. The rmsd between Cα atoms of the dimers (residues 11−101 of each monomer) was 0.61 Å. Panel C shows a ribbon diagram of the DCoH2 homotetramer. The saddle-shaped dimers (above and below, with each monomer colored cyan and blue) interact primarily through helix 2 of each monomer (residues 44−59, magenta) to form the tetramer. This helix, called the recognition helix (*8*), also forms the interface for HNF1. A small dimer−dimer contact also occurs between the C-terminal residues (residues 102 and 103, magenta). Contact residues were defined as being within 4 Å of the neighboring dimer. As shown in panel D, a water molecule is buried at the center of the DCoH2 tetramer interface (blue). $F_o - F_c$ difference electron density (3σ) for the water molecule is shown with the water deleted from the model. The water forms hydrogen bonds to four Ser51 side chains, one from each DCoH2 monomer. Two rotamers are seen for each Ser51 side chain. Distances are indicated to the serine side chain closest to the water molecule. No analogous water is seen in the DCoH1 tetramer (orange) because the larger Thr51 side chains fills the equivalent space and the Thr51 hydroxyl groups are not positioned correctly.

mobility. In contrast, coexpression of either DCoH protein stabilized preformed HNF1α dimers. Thus, DCoH2 inhibited the exchange of subunits in HNF1α dimers in vitro.

Comparison of DCoH2 and DCoH1 Structures. We determined the high-resolution crystal structure of DCoH2 to explore the basis for its biochemical properties. DCoH2 crystallized with a dimer in the asymmetric unit, and the structure was solved by molecular replacement using a DCoH dimer as the search model. The refined DCoH2 structure gave R/R_{free} values of 0.215/0.236 for all data to 1.6 Å resolution (Table 1, Figure 4A). The DCoH2 and DCoH1 dimers adopt the same fold with a root-mean-square deviation (rmsd) for the Cα atoms of 0.61 Å (residues 11−101 in each monomer, Figure 4B). A DCoH2 tetramer similar to the DCoH1 tetramer is generated through a crystallographic 2-fold rotation axis (Figure 4C). The DCoH2 dimer−dimer interaction is similar to that of DCoH1 with a Cα rmsd between the tetramers of 0.80 Å (residues 11−101 of each monomer). The interaction surface consists primarily of helix 2, residues 44−60, from each monomer. Upon tetramerization, 2434 Å^2 in DCoH2 and 2860 Å^2 in DCoH1 are buried. The difference in the buried surface area is primarily due to contacts between the C-termini; the C-terminus of one DCoH2 monomer is disordered in the crystal structure. Three sequence differences occur in the respective recognition helices of DCoH2 and DCoH1: Gln45Arg, Ser51Thr, and Asn61Asp (Figure 5A,E). The tetramers conserve the hydrophobic core but show altered H-bonding interactions. The major difference at the interface of the recognition helices occurs at position 51, which is a serine in DCoH2 and a threonine in DCoH1. A water molecule is buried in the DCoH2 tetramer interface by interacting with the four Ser51 residues from each monomer (Figure 4D). The bulkier Thr51 of DCoH1 prevents binding of this water molecule.

Most of the 32 side chain differences between the two DCoH paralogs are located on the protein surface (Figure 5). A number of regions are conserved among all vertebrate DCoH1 and DCoH2 sequences, including the recognition helix (Figure 5A,E), and patches of residues in the saddle (Figure 5D,H) and on the "sides" of the saddle (Figure 5B,C,F,G). Other surface residues are distinct to the DCoH1 and DCoH2 subfamilies. Overall, the surface of DCoH1 is more highly conserved among orthologs than that of DCoH2.

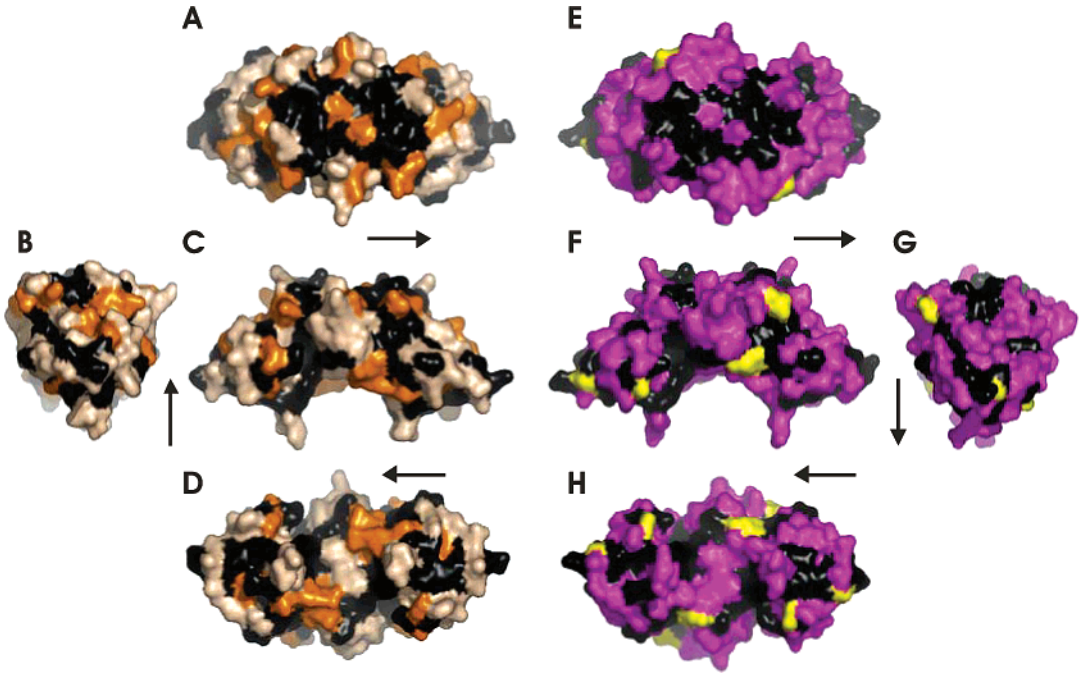

FIGURE 5: Surface conservation patterns in the vertebrate DCoH2 (A−D) and DCoH1 (E−H) dimers. Colors indicate sequence conservation within the DCoH2 subfamily only (orange) or DCoH1 subfamily only (magenta), or within both DCoH1 and DCoH2 (black). Tan indicates residues not conserved within the DCoH2 subfamily; yellow indicates residues not conserved within the DCoH1 subfamily. Models A and E are viewed from the "top" (above the recognition helices). Most residues in helix 2 are conserved in both DCoH1 and DCoH2, except for residue 51, which is a serine in DCoH2 (A) and a threonine in DCoH1 (E). Models C and F show "side" views; models B and G show "front" views. Models D and H show views facing into the saddle. Each view is derived from the "side" views (models C and F) by a right-handed 90° rotation around the indicated axis. DCoH1 is more highly conserved than DCoH2. The "stirrups" and several surface residues, including in the saddle, distinguish the DCoH1 and DCoH2 subfamilies. This figure is based on the four species, human, mouse, rat, and chicken, known to encode both DCoH1 and DCoH2 paralogs. Conservation is defined according to similarity groups (FYW, IVLM, RK, DE, GA, TS, NQ, single letter amino acid code) except where residues are identical in DCoH1 or DCoH2 subfamilies and distinct from the other subfamily (e.g., both serine and threonine are found at residue 51 in DCoH2, Thr51 is conserved in DCoH1). The solvent-exposed surfaces were drawn using PyMol (Delano, W. L. (2002) *The PyMol Molecular Graphics System*, http://www.pymol.org).

The "stirrups" are distinct within each subfamily (Figure 5C,F).

DISCUSSION

As demonstrated for the nuclear hormone receptor superfamily (reviewed in *39*), diverse regulatory outcomes can be achieved through the interaction of transcription factors with multiple coactivators and corepressors. Here we compared the properties of two paralogs of the coactivator DCoH to test the idea that they fulfill distinct functional roles that may account for the phenotypes of DCoH1 knockout mice. The DCoH1 and DCoH2 subfamilies are more highly conserved from mice to humans than they are between each other, suggesting that their functions may have diverged. Table 2 summarizes a comparison between DCoH1 and DCoH2 paralogs. DCoH interacts specifically with the small family of HNF1 transcription factors comprising isoforms of HNF1α and HNF1*β*. DCoH1 null mice retained significant HNF1α activity and a degree of phenylalanine hydroxylase activity, suggesting that DCoH2 partially complements the coactivator function of DCoH1 in vivo (*19*).

To determine the number of DCoH paralogs in humans, we searched the human genome using tblastn (www.ncbi.nlm.nih.gov/BLAST/). The search identified four sequences related to DCoH (Table 3): the annotated *DCoH* gene on chromosome 10 (DCoH1), the annotated muscle *DCoH* on chromosome 5 (DCoH2), and two pseudogenes on chromosomes 2 and 17. The exon structures of *DCoH1* and *DCoH2* are identical. These gene structures were confirmed by Genscan. The sequence on chromosome 17 is located in intron 5 of the annotated CARKL gene. The DCoH coding region contains a frame shift at position 30 and stop codons at positions 8 and 70. The sequence on chromosome 2 contains two regions of low homology with DCoH2. Exon 2 of this aligned sequence contains a stop codon. In contrast with the expressed DCoH genes, the exon structures of the pseudogenes predicted by Genscan did not agree with the exons predicted from the alignment with DCoH.

These DCoH paralogs were the only two identified among vertebrates in an exhaustive PSI-BLAST search of the nonredundant database. This search yielded 42 sequences with significant homology to DCoH1 and DCoH2. These homologues included eukaryotic (*18*), prokaryotic (*20*), and archaeal (*4*) sequences (Figure 6). DCoH is highly conserved among metazoans: the human DCoH1 sequence is identical to the rat sequence and 55% identical to the *Drosophila melanogaster* sequence. Two DCoH paralogs were found in human, rat, mouse, and chicken, forming two distinct branches of the phylogenetic tree. Only a single DCoH gene was found in nonvertebrate metazoans.

The nonmetazoan sequences cluster into three general groups, named after the most abundant sequences in that branch: the α/*β*-proteobacteria, the archaeal/Actinobacteria, and the *γ*-proteobacteria. The most highly conserved residues correspond to the active site of DCoH1: Glu58, Asp61, His62, His63, Ser78, His80, Glu81, and Asp89 (*12*). Only

Table 2: Comparison between DCoH1 and DCoH2 Paralogs

property	DCoH1	DCoH2
human gene locus	10q22	5q31.2
conservation, percent identity	mouse vs human, 99%	mouse vs human, 88%
	human DCoH1 vs human DCoH2, 61%	
dehydratase activity	complementation assay (*22*, *38*) in vitro activity assay (*1*)	complementation assay (Figure 3A)
binding to HNF1 in vivo	EMSA Co−IP (*6*)	EMSA (Figure 3B) Co−IP (Figure 3C)
binding to HNF1 in vitro	no	EMSA supershift (Figure 3D) pull-down assay (Figure 3E)
stabilizing HNF1 dimer	competition assay (*6*)	competition assay (Figure 3F)
coactivator activity	transient transfection assay (*6*)	transient transfection assay (*21*)
homotetramer stability	hyperstable: complex with HNF1 requires co-folding (*14*, *15*) melting temperature > 90° (*40*)	increased dissociation rate: complex with HNF1 upon mixing (Figure 3D,E)
tetramerization interface	T51 at center of hydrophobic interface (*11*)	S51 and ordered water at hydrophobic interface (Figure 4D)
expression	liver, kidney, intestine, stomach, pancreas; low in skin, eye and brain (*6*, *19*, *41*)	intestine, muscle; low in kidney and liver (*19*, *21*)
interactions	unknown	Dyrk1B kinase (*21*)

Table 3: The Human Genome Contains Two DCoH Paralogs and Two Pseudogenes[a]

chromosome/ accession number	predicted exons	alignment	*E* value	Genscan identified exons	*P*
10/NT_008583.13	1	promoter to Met1[b]	*d*	63bp-Met1	0.565
	2	2−45[b]	6×10^{19}	2−45	0.997
	3	46−72[b]	1×10^{9}	46−72	0.977
	4	73−104[b]	2×10^{10}	73−104	0.950
5/NT_034776.2	1	promoter to Met1[c]	*d*		
	2	2−45[c]	2×10^{17}	2−45	0.479
	3	46−72[c]	3×10^{10}	46−72	0.468
	4	73−103[c]	2×10^{9}	73−103	0.469
17/NT_010692.9	1	1−43[c]	2×10^{9}		
	2	33−103[c]	1×10^{11}		
2/NT_005403.11	1	17−47[c]	3×10^{4}		
	2	59−100[c]	0.001		

[a] The *E* values from the tblastn alignment and the *P* values from Genscan (Burge, C. B., http://genes.mit.edu/GENSCAN.html) are shown. [b] Alignment with human DCoH1. [c] Alignment with mouse DCoH2. [d] Not applicable.

four sequences (from *Streptomyces coelicolor*, *Leishmania major*, *Vibrio cholerae*, and *Aribidopsis thaliana*) lack the characteristic His62-His63-Pro64 tripeptide. This conservation suggests that the enzymatic function of DCoH predates the transcriptional function.

In mammals, DCoH catalyzes the dehydration of pterin-4α-carbinolamine, the first step in recycling tetrahydrobiopterin. The fully reduced tetrahydrobiopterin is an essential cofactor for the aromatic amino acid hydroxylases and the three nitric oxide synthases. It is generally accepted that bacteria lack tetrahydrobiopterin (*42*, *43*). Nevertheless, bacterial homologues of mammalian phenylalanine hydroxylase (PAH) and nitric oxide synthase (NOS) have been identified. PAH has been reported in both α and γ divisions of *Proteobacteria* (*38*) with similar folds to the mammalian proteins (*44*). Bacterial PAH can utilize tetrahydrobiopterin as a cofactor in vitro (*45*). The NOS fold has been conserved as well, as demonstrated by the structure of a *Staphylococcus aureus* homologue of the oxygenase domain of mammalian NOS (*46*). Bacterial NOS lacks the reductase domain of the mammalian counterpart. A bacterial oxygenase fused to a mammalian reductase domain from neuronal NOS can use tetrahydrobiopterin or tetrahydrofolate to generate NO (*47*, *48*). While the authentic cofactors are unknown for the bacterial enzymes, pteridine derivatives do function as cofactors in other electron-transfer reactions in prokaryotes and archaeabacteria (*43*). The conservation of the active site in all DCoH homologues suggests that the PCD activity may play roles in recycling pterin cofactors in all kingdoms of life.

The functional and phylogenetic evidence suggests that adaptation of the helical surface of the DCoH dimer for protein−protein interactions evolved after the enzymatic function (Figure 4C). The transcriptional coactivator function of DCoH appears to be unique to vertebrates. DCoH enhances the activity of the HNF1 transcription factors, which are unique to vertebrates (*49*). There are indications that DCoH may interact with a second vertebrate transcription factor (*10*, *50*−*53*). No evidence for a transcriptional role for DCoH in prokaryotes has been found (*38*). The prokaryotic DCoH is dimeric, as demonstrated by the *P. aeruginosa* PhhB structure, indicating that a DCoH dimer is enzymatically active (*54*). The recent structure of DCoH from *Thermus thermophilus* (RCSB Protein Data Bank ID 1USO) (*55*) indicates that the archaeal homologues are dimers.[2] The rmsd between Cα atoms of the archaeal and mouse dimers (residues 12−75 from both monomers of *T. thermophilus* DCoH aligned with 34−97 from both monomers of mouse DCoH2) was 1.6 Å.

The interface that mediates tetramer formation in vertebrate DCoH proteins is composed primarily of residues from helix 2, residues 43−59, which we will refer to as the recognition helix (*11*). This same interface interacts with HNF1α (*8*). In contrast to the active site residues, the recognition helices are not conserved across the kingdoms of life. While tetramerization does not interfere with the enzymatic activity of DCoH, it does compete with HNF1 binding (*8*). The implication is that tetramerization coevolved with the

[2] The helical surface of the *T. thermophilus* DCoH dimer forms a crystal packing interaction that is distinct from the vertebrate DCoH tetramer, suggesting that it is not biologically relevant.

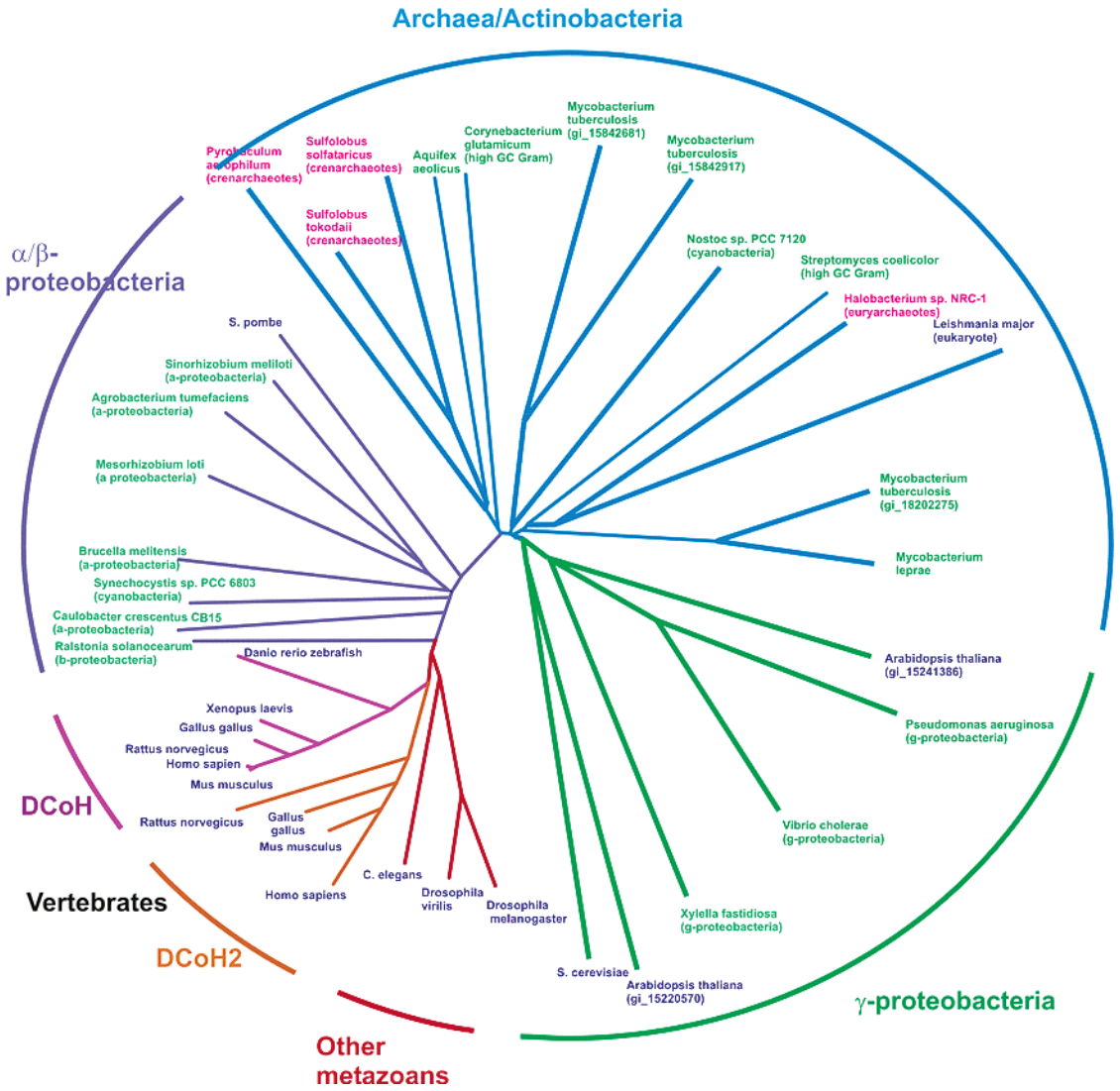

FIGURE 6: Phylogenetic relationship of DCoH sequences. An unrooted tree of 42 DCoH homologues shows that the vertebrate DCoH1 (violet branches) and DCoH2 (orange branches) sequences form distinct subfamilies. Five metazoan genomes contain only a single known DCoH gene: *X. laevis*, *Danio rerio*, *Caenorhabditis elegans*, *Drosophila virilis*, *and Drosophila melanogaster*. The remaining sequences clustered into three main branches: the α/*β* proteobacteria (purple branches), the archaeal/Actinobacteria (blue branches), and the *γ* proteobacteria (green branches). These subfamilies were named according to the most abundant known members. The color of the text signifies the kingdom of the organism: eukaryotic (purple), prokaryotic (green), and archaeal (magenta).

transcriptional function of DCoH, and homotetramer formation contributes to the regulation of coactivation by DCoH. DCoH2, like DCoH1, forms homotetramers in solution. Conservation of the tetramerization interface suggests the possibility of mixed DCoH1/DCoH2 tetramers. Coexpression of DCoH1 and DCoH2 confirmed that they were capable of forming mixed tetramers and may do so in vivo.

The structure of DCoH2 is consistent with the functional similarities and differences compared to DCoH1. We demonstrated that DCoH2, like DCoH1, recycles 4α-hydroxytetrahydrobiopterin and binds HNF1α dimers. DCoH2 exhibits a number of properties that may distinguish it functionally from DCoH1. The expression pattern of DCoH2 differs from that of DCoH1. For example, DCoH2 has recently been identified in skeletal muscle (*21*), which does not contain DCoH1 (*6*, *56*). DCoH1 and DCoH2 may interact with distinct sets of factors, since the sequence differences map primarily to the protein surfaces (Figure 5). The saddle of DCoH, which presents a large concave surface suitable for protein−protein interactions, is lined with different residues in the DCoH1 and DCoH2 subfamilies. Mutagenesis studies suggest that the coactivator function of DCoH involves recruitment of additional factors to the DCoH saddle (*15*). A candidate for a paralog-specific interacting protein is the serine/threonine kinase Mirk, which has been shown to interact with DCoH2 (*21*).

Although both DCoH1 and DCoH2 can interact with HNF1α, they differ in their availability for HNF1 binding (Figure 3). The DCoH dimer, and not the tetramer, associates with HNF1α. Our in vitro studies suggest that the DCoH2 tetramer is less stable than the DCoH1 tetramer, allowing it to dissociate into dimers that interact with HNF1α in solution. In contrast, formation of the DCoH1/HNF1α complex requires cofolding of the two proteins. The hyperstable DCoH1 tetramer sequesters the HNF1α binding surface. The primary sequence difference between DCoH2 and DCoH1 in the recognition helix is at residue 51, which is a threonine in DCoH1 and a serine in DCoH2. The smaller serine side chain allows binding of a buried water molecule upon DCoH2 homotetramerization. Water burial and ordering

are unfavorable (*57*−*60*), and this effect would be expected to facilitate DCoH2/HNF1 complex formation. As a result, DCoH2 may preferentially associate with HNF1α, instead of forming stable homotetramers. The relative instability of DCoH2 homotetramers may account for the low levels of cytoplasmic DCoH2 activity and the predominant nuclear association of DCoH2 with HNF1 observed in *DCoH1* null mice (*19*).

The human DCoH2 sequence also encodes serine at residue 51 suggesting a less stable homotetramer than human DCoH1, similar to mouse. It remains to be seen whether decreased homotetramer stability is a property that distinguishes DCoH2 from DCoH1 in general. While both *Gallus gallus* and *Rattus norvegicus* DCoH2 sequences contain Thr51, they each possess nonconserved residues elsewhere in the recognition helix composing the tetramerization interface (at Asn59 and Val55, respectively) that may destabilize the homotetramer. Alternatively, these variants may alter the stability of the DCoH/HNF1 complex, since the same surface forms the interface with HNF1.

The decreased stability of the DCoH2 homotetramer relative to DCoH1 may underlie normal functional differences between the two paralogs. We have proposed that homotetramerization of DCoH1 autoinhibits coactivator function by inhibiting HNF1α binding (*8*). The phylogenetic data support the idea that tetramerization of DCoH coevolved with the coactivator function of DCoH. Thus, DCoH1 may function as a timer in which coactivator function is regulated kinetically. The dissociation rate of the DCoH1/HNF1 complex would determine the lifetime of the coactivator complex if the DCoH1 tetramer acts as a stable sink that lowers the concentration of DCoH1 dimers. In contrast, the less stable DCoH2 tetramer may provide a thermodynamic switch that affords more rapid changes in coactivator activity. Further experiments are required to test this model.

ACKNOWLEDGMENT

We thank James Holton for assistance in data collection and data processing. X-ray data were collected at Beamline 5.0.2 at the Lawrence Berkeley National Laboratory Advanced Light Source. The Advanced Light Source is supported by the Director, Office of Science, Office of Basic Energy Sciences, Materials Sciences Division, of the U.S. Department of Energy under Contract No. DE-AC03-76SF00098. We thank George Johnen for supplying rabbit anti-DCoH antibody.

SUPPORTING INFORMATION AVAILABLE

A list of 42 aligned DCoH sequences identified using PSI-BLAST, which was used to generate the phylogenetic tree (Figure 6). This material is available free of charge via the Internet at http://pubs.acs.org.

REFERENCES

1. Citron, B., Davis, M., Milstien, S., Gutierrez, J., Mendel, D., Crabtree, G., and Kaufman, S. (1992) Identity of 4a-carbinolamine dehydratase, a component of the phenylalanine hydroxylation system, and DCoH, a transregulator of homeodomain proteins, *Proc. Natl. Acad. Sci. U.S.A. 89*, 11891−11894.
2. Hauer, C., Rebrin, I., Thony, B., Neuheiser, F., Curtius, H., Hunziker, P., Blau, N., Ghisla, S., and Heizmann, C. (1993) Phenylalanine hydroxylase-stimulating protein/pterin-4α-carbinolamine dehydratase from rat and human liver. Purification, characterization, and complete amino acid sequence, *J. Biol. Chem.* 4828−4831.
3. Citron, B., Kaufman, S., Milstien, S., Naylor, E., Greene, C., and Davis, M. (1993) Mutation in the 4a-carbinolamine dehydratase gene leads to mild hyperphenylalaninemia with defective cofactor metabolism, *Am. J. Hum. Genet. 53*, 768−774.
4. Thony, B., Neuheiser, F., Kierat, L., Blaskovics, M., Arn, P., Ferreira, P., Rebrin, I., Ayling, J., and Blau, N. (1998) Hyperphenylalaninemia with high levels of 7-biopterin is associated with mutations in the PCBD gene encoding the bifunctional protein pterin-4a-carbinolamine dehydratase and transcriptional coactivator (DCoH), *Am. J. Hum. Genet. 62*, 1302−1311.
5. Schallreuter, K., Wood, J., Pittelkow, M., Gutlich, M., Lemke, K., Rodl, W., Swanson, N., Hitzemann, K., and Ziegler, I. (1994) Regulation of melanin biosynthesis in the human epidermis by tetrahydrobiopterin, *Science 263*, 1444−1446.
6. Mendel, D., Khavari, P., Conley, P., Graves, M., Hansen, L., Admon, A., and Crabtree, G. (1991) Characterization of a cofactor that regulates dimerization of a mammalian homeodomain protein, *Science 254*, 1762−1767.
7. Yamagata, K., Furuta, H., Oda, N., Kaisaki, P., Menzel, S., Cox, N., Fajans, S., Signorini, S., Stoffel, M., and Bell, G. (1996) Mutations in the hepatocyte nuclear factor-1α gene in maturity-onset diabetes of the young (MODY3), *Nature 384*, 455−458.
8. Rose, R., Bayle, J., Endrizzi, J., Cronk, J., Crabtree, G., and Alber, T. (2000) Structural basis of dimerization, coactivator recognition and MODY3 mutations in HNF-1α, *Nat. Struct. Biol. 7*, 744−748.
9. Eskinazi, R., Thony, B., Svoboda, M., Robberecht, P., Dassesse, D., Heizmann, C., Van Laethem, J., and Resibois, A. (1999) Overexpression of pterin-4a-carbinolamine dehydratase/dimerization cofactor of hepatocyte nuclear factor 1 in human colon cancer, *Am. J. Pathol. 155*, 1105−1113.
10. von Strandmann, E., Senkel, S., Ryffel, G., and Hengge, U. (2001) Dimerization co-factor of hepatocyte nuclear factor 1/pterin-4α-carbinolamine dehydratase is necessary for pigmentation in Xenopus and overexpressed in primary human melanoma lesions, *Am. J. Pathol. 158*, 2021−2029.
11. Endrizzi, J., Cronk, J., Wang, W., Crabtree, G., and Alber, T. (1995) Crystal structure of DCoH, a bifunctional, protein-binding transcriptional coactivator, *Science 268*, 556−559.
12. Cronk, J., Endrizzi, J., and Alber, T. (1996) High-resolution structures of the bifunctional enzyme and transcriptional coactivator DCoH and its complex with a product analogue, *Protein Sci. 5*, 1963−1972.
13. Rose, R., Endrizzi, J., Cronk, J., Holton, J., and Alber, T. (2000) High-resolution structure of the HNF-1α dimerization domain, *Biochemistry 39*, 15062−15070.
14. Ficner, R., Sauer, U., Stier, G., and Suck, D. (1995) Three-dimensional structure of the bifunctional protein PCD/DCoH, a cytoplasmic enzyme interacting with transcription factor HNF1, *EMBO J. 14*, 2034−2042.
15. Johnen, G., and Kaufman, S. (1997) Studies on the enzymatic and transcriptional activity of the dimerization cofactor for hepatocyte nuclear factor 1, *Proc. Natl. Acad. Sci. U.S.A. 94*, 13469−13474.
16. Pontoglio, M., Sreenan, S., Roe, M., Pugh, W., Ostrega, D., Doyen, A., Pick, A., Baldwin, A., Velho, G., Froguel, P., Levisetti, M., Bonner-Weir, S., Bell, G., Yaniv, M., and Polonsky, K. (1998) Defective insulin secretion in hepatocyte nuclear factor 1α-deficient mice, *J. Clin. Invest. 101*, 2215−2222.
17. Pontoglio, M., Barra, J., Hadchouel, M., Doyen, A., Kress, C., Bach, J., Babinet, C., and Yaniv, M. (1996) Hepatocyte nuclear factor 1 inactivation results in hepatic dysfunction, phenylketonuria and renal Fanconi syndrome, *Cell 84*, 575−585.
18. Lee, Y., Sauer, B., and Gonzalez, F. (1998) Laron dwarfism and non-insulin-dependent diabetes mellitus in the Hnf-1α knockout mouse, *Mol. Cell. Biol. 18*, 3059−3068.
19. Bayle, J., Randazzo, F., Johnen, G., Kaufman, S., Nagy, A., Rossant, J., and Crabtree, G. (2002) Hyperphenylalaninemia and impaired glucose tolerance in mice lacking the bifunctional DCoH gene, *J. Biol. Chem. 277*, 28884−28891.
20. Kim, H., You, S., Foster, L., Farris, J., Choi, Y., and Foster, D. N. (2001) Differential expression of chicken dimerization cofactor of hepatocyte nuclear factor-1 (DCoH) and its novel counterpart, DCoHα, *Biochem. J. 354*, 645−653.
21. Lim, S., Jin, K., and Friedman, E. (2002) Mirk protein kinase is activated by MKK3 and functions as a transcriptional activator of HNF1α, *J. Biol. Chem. 277*, 25040−25046.

22. Zhao, G., Xia, T., Song, J., and Jensen, R. A. (1994) *Pseudomonas aeruginosa* possesses homologues of mammalian phenylalanine hydroxylase and 4α-carbinolamine dehydratase/DCoH as part of a three-component gene cluster, *Proc. Natl. Acad. Sci. U.S.A. 91*, 1366−1370.
23. Lassar, A. B., Davis, R. L., Wright, W. E., Kadesch, T., Murre, C., Voronova, A., Baltimore, D., and Weintraub, H. (1991) Functional activity of myogenic HLH proteins requires hetero-oligomerization with E12/E47-like proteins in vivo, *Cell 66*, 305−315.
24. Tomei, L., Cortese, R., and De Francesco, R. (1992) A POU-A related region dictates DNA binding specificity of LFB1/HNF1 by orienting the two XL-homeodomains in the dimer, *EMBO J. 11*, 4119−4129.
25. Leslie, A. (1992) Recent changes to the MOSFLM package for processing film and image plate data, *Joint CCP4 ESF-EAMCB Newslett. Protein Crystallogr.* No. 26.
26. Holton, J., and Alber, T. (2003) Automated protein crystal structure determination using ELVES, *Proc. Natl. Acad. Sci. U.S.A. 101*, 1537−1542.
27. Evans, P. R. (1993) Data Reduction, *Proc. CCP4 Study Weekend Data Collect. Process.*, 114−122.
28. French, G., and Wilson, K. (1978) On the treatment of negative intensity observations, *Acta Crystallogr. A34*, 517.
29. Collaborative Computation Project, N. (1994) The CCP4 suite: programs for protein crystallography, *Acta Crystallogr. D50*, 760−763.
30. Brunger, A., Adams, P., Clore, G., Delano, W., Gros, P., Grosse-Kunstleve, R., Jiang, J.-S., Kuszewski, J., Nilges, N., Pannu, N., Read, R., Rice, L., Simonson, T., and Warren, G. (1998) Crystallography and NMR system (CNS): a new software system for macromolecular structure determination, *Acta Crystallogr. D54*, 905−921.
31. Perrakis, A., Sixma, T., Wilson, K., and Lamzin, V. (1997) wARP: improvement and extension of crystallographic phases by weighted averaging of multiple refined dummy atomic models, *Acta Crystallogr. D53*, 448−455.
32. Lamzin, V., and Wilson, K. (1993) Automated refinement of protein models, *Acta Crystallogr. D49*, 129−149.
33. Jones, T., Zhou, J., Cowan, S., and Kjeldgaard, M. (1991) Improved methods for building protein models in electron density maps and the location of errors in these models, *Acta Crystallogr. A47*, 110−119.
34. Altschul, S., Madden, T., Schaffer, A., Zhang, J., Zhang, Z., Miller, W., and Lipman, D. (1997) Gapped BLAST and PSI-BLAST: a new generation of protein database search programs, *Nucleic Acids Res. 25*, 3389−3402.
35. Felsenstein, J. (1993) *PHYLIP (Phylogeny Inference Package*), version 3.5c, Distributed by the author, Department of Genetics, University of Washington, Seattle, WA.
36. Burge, C., and Karlin, S. (1997) Prediction of complete gene structures in human genomic DNA, *J. Mol. Biol. 268*, 78−94.
37. Thompson, J. D., Higgins, D. G., and Gibson, T. J. (1994) CLUSTAL W: improving the sensitivity of progressive multiple sequence alignment through sequence weighting, position-specific gap penalties and weight matrix choice, *Nucleic Acids Res. 22*, 4673−4680.
38. Song, J., Xia, T., and Jensen, R. (1999) PhhB, a *Pseudomonas aeruginosa* homologue of mammalian pterin 4a-carbinolamine dehydratase/DCoH, does not regulate expression of phenylalanine hydroxylase at the transcriptional level, *J. Bacteriol. 181*, 2789−2796.
39. Aranda, A., and Pascual, A. (2001) Nuclear hormone receptors and gene expression, *Physiol. Rev. 81*, 1269−1304.
40. Cronk, J. (1996) Structural studies of DCoH, a bifunctional enzyme and protein-binding transcriptional coactivator, Ph.D. Thesis, University of California, Berkeley, Berkeley, CA.
41. Lei, X. D., Woodworth, C. D., Johnen, G., and Kaufman, S. (1997) Expression of 4α-carbinolamine dehydratase in human epidermal keratinocytes, *Biochem. Biophys. Res. Commun. 238*, 556−559.
42. Werner-Felmayer, G., Golderer, G., and Werner, E. (2002) Tetrahyderobiopterin biosynthesis, utilization and pharmacological effects, *Curr. Drug Metab. 3*, 159−173.
43. Kadish, K., Smith, K., and Guilard, R. (2000) *The Porphyrin Handbook*, Academic Press, London.
44. Erlandsen, H., Kim, J., Patch, M., Han, A., Volner, A., Abu-Omar, M., and Stevens, R. (2002) Structural comparison of bacterial and human iron-dependent phenylalanine hydroxylases: similar fold, different stability and reaction rates, *J. Mol. Biol. 320*, 645−661.
45. Chen, D., and Frey, P. (1998) Phenylalanine hydroxylase from *Chromobacterium violaceum*, *J. Biol. Chem. 273*, 25594−25601.
46. Bird, L., Ren, J., Zhang, J., Foxwell, N., Hawkins, A., Charles, I., and Stammers, D. (2002) Crystal structure of SANOS, a bacterial nitric oxide synthase oxygenase protein from *Staphylococcus aureus*, *Structure 10*, 1687−1696.
47. Adak, S., Aulak, K., and Stuehr, D. (2002) Direct evidence for nitric oxide production by a nitric oxide synthase-like protein from *Bacillus subtilis*, *J. Biol. Chem. 277*, 16167−16171.
48. Adak, S., Bilwes, A., Panda, K., Hosfield, D., Aulak, K., McDonald, J., Tainer, J., Getzoff, E., Crane, B., and Stuehr, D. (2002) Cloning, expression, and characterization of a nitric oxide synthase protein from *Deinococcus radiodurans*, *Proc. Natl. Acad. Sci. U.S.A. 99*, 107−112.
49. Deryckere, F., Byrnes, L., Wagner, A., McMarrow, T., and Gannon, F. (1995) Salmon HNF1: cDNA sequence, evolution, tissue specificity and binding to the salmon serum albumin promoter, *J. Mol. Biol. 247*, 1−10.
50. Resibois, A., Cuvelier, L., Svoboda, M., Heizmann, C., and Thony, B. (1999) Immunohistochemical localisation of pterin-4alpha-carbinolamine dehydratase in rat peripheral organs, *Histochem. Cell Biol. 111*, 381−390.
51. Pogge v Strandmann, E., and Ryffel, G. (1995) Developmental expression of the maternal protein XDCoH, the dimerization cofactor of the homeoprotein LFB1 (HNF1), *Development 121*, 1217−1226.
52. Pogge v Strandmann, E., Senkel, S., and Ryffel, G. (2000) Ectopic pigmentation in Xenopus in response to DCoH/PCD, the cofactor of HNF1 transcription factor/pterin-4alpha-carbinolamine dehydratase, *Mech. Dev. 91*, 53−60.
53. Strandmann, E., Senkel, S., and Ryffel, G. (1998) The bifunctional protein DCoH/PCD, a transcription factor with a cytoplasmic enzymatic activity, is a maternal factor in the rat egg and expressed tissue specifically during embryogenesis, *Int. J. Dev. Biol. 42*, 53−59.
54. Suck, D., and Ficner, R. (1996) Structure and function of PCD/DCoH, an enzyme with regulatory properties, *FEBS Lett. 389*, 35−39.
55. Tahirov, T., and Inagaki, E. DCoH, a bifunctional protein-binding transcriptional coactivator, Pro9Leu mutant, to be published.
56. Davis, M. D., Kaufman, S., and Milstien, S. (1992) Distribution of 4a-hydroxytetrahydropterin dehydratase in rat tissues. Comparison with the aromatic amino acid hydroxylases, *FEBS Lett. 302*, 73−76.
57. Timasheff, S. (1992) Water as ligand: preferential binding and exclusion of denaturants in protein unfolding, *Biochemistry 31*, 9857−9864.
58. Fischer, S., and Verma, C. (1999) Binding of buried structural water increases the flexibility of proteins, *Proc. Natl. Acad. Sci. U.S.A. 96*, 9613−9615.
59. Lam, P., Jadhav, P., Eyermann, C., Hodge, C., Ru, Y., Bacheler, L., Meek, J., Otto, M., Rayner, M., Wong, Y., Chang, C., Weber, P., Jackson, D., Sharpe, T., and Erickson-Viitanen, S. (1994) Rational design of potent, bioavailable, nonpeptide cyclic ureas as HIV protease inhibitors, *Science 263*, 380−384.
60. Dunitz, J. (1994) The entropic cost of bound water in crystals and biomolecules, *Science 264*, 670.

BI049620T